

Rigid amorphous fraction and melting behavior of poly(ethylene terephthalate)

Maria Cristina Righetti · Michele Laus ·
Maria Laura Di Lorenzo

Received: 6 February 2014 / Revised: 28 February 2014 / Accepted: 10 March 2014 / Published online: 26 March 2014
© Springer-Verlag Berlin Heidelberg 2014

Abstract The multiple melting behavior of poly(ethylene terephthalate) (PET) is generally attributed to the fusion of original crystals recrystallized during the heating at conventional scanning rate. In the present study, the triple and double melting behavior that is observed after isothermal crystallization at T_c lower and higher than 215 °C, respectively, is put in relation with the presence and absence of rigid amorphous fraction around the original primary crystal lamellae. The complex melting behavior is explained by assuming that two different morphologies of primary crystals develop during crystallization at temperatures lower than 215 °C, in a proportion that is a function of the crystallization temperature: chain cluster aggregations with a high percentage of rigid amorphous fraction on the boundaries and small crystals with a high percentage of adjacent reentry folding and reduced constraints at the amorphous/crystal interphase. These distinct morphologies differently transform upon heating at low scanning rate, originating two endotherms. On the contrary, after crystallization at $T_c > 215$ °C, all the primary crystalline structure, which probably are characterized by the same morphology made of tightly chain folded lamellae and absence of rigid amorphous fraction, undergo the same reorganization route, originating a single endotherm.

Keywords Rigid amorphous fraction · Interphase · Chain mobility · Temperature-modulated calorimetry

Introduction

The common description of semicrystalline polymers as constituted by two separate phases, amorphous and crystalline, has been recently replaced by a more complete one that takes into account also the intermediate nanophase present at the interface between the crystalline and the surrounding amorphous regions [1]. The decoupling between crystalline and amorphous phases is in general incomplete, due to the length of the polymer molecules, which is much higher than the dimensions of the crystalline phase, at least in one direction. The interphase between crystalline and amorphous regions is non-crystalline and includes amorphous chain portions whose mobility is hindered by the near crystalline structures [2]. This interphase is generally named “rigid amorphous fraction” (RAF), its mobility being lower than that of the unconstrained amorphous phase, which is usually addressed as “mobile amorphous fraction” (MAF).

A detailed knowledge of the nanoscale phase behavior of semicrystalline polymer materials is decisive for the assessment of mechanical, thermal, gas permeability, and other macroscopic properties [3–8]. By acting as stress transfer point, the RAF produces an increase in the elastic modulus, with a behavior similar to that of the crystal phase [3, 4, 7]. The rigid amorphous fraction affects also the barrier properties, due to its higher free volume with respect to the mobile amorphous region, which results in a different diffusion rate of small molecules [5–8].

The relationship between crystal growth and rigid amorphous fraction development and between melting and rigid amorphous fraction mobilization has been detailed in the literature only for a limited number of semicrystalline

M. C. Righetti (✉)
Istituto per i Processi Chimico-Fisici, Consiglio Nazionale delle
Ricerche, INSTM, UdR Pisa, Via G. Moruzzi 1, 56124 Pisa, Italy
e-mail: cristina.righetti@ipcf.cnr.it

M. Laus
Dipartimento di Scienze e Innovazione Tecnologica,
Università del Piemonte Orientale ‘A. Avogadro’, INSTM,
UdR Alessandria, Viale T. Michel 11, 15121 Alessandria, Italy

M. L. Di Lorenzo
Istituto per i Polimeri, Compositi e Biomateriali,
Consiglio Nazionale delle Ricerche,
c/o Comprensorio Olivetti, Via Campi Flegrei 34,
80078 Pozzuoli (NA), Italy

polymers [9–18]. These studies, conducted independently of one another, in different crystallization and melting conditions and with different methods of data processing, if combined and compared with each other, prove that the different thermal histories affect the combined evolution and disappearance of crystalline and rigid amorphous phases. During crystallization of poly(ethylene terephthalate) (PET), poly[(R)-3-hydroxybutyrate] (PHB), and bisphenol-A polycarbonate (PC) at temperatures slightly above the respective T_g 's, vitrification of the rigid amorphous fraction parallels crystal growth [9, 10, 14], whereas in isotactic polystyrene (iPS) crystallized at 140 °C and 170 °C, i.e. well above the bulk T_g , the rigid amorphous fraction increases markedly after spherulite impingement, which corresponds to the beginning of crystallization in restricted regions [11, 12]. Upon slow cooling from the melt, both in iPS and PET, RAF vitrification takes place during the final stages of the non-isothermal crystallization process, with the full establishment of the rigid amorphous structure completed during the subsequent cooling to room temperature [13, 15]. Conversely, a much slower cooling rate from the melt, attained with quasi-isothermal step cooling, results in vitrification of the RAF in PET and poly(trimethylene terephthalate) mainly after conclusion of the crystallization [16, 17].

The influence of the crystallization temperature on the RAF development was systematically investigated for poly(L-lactic acid) (PLLA) and poly[(R)-3-hydroxybutyrate] (PHB) [19–21]. Both in PLLA and PHB, rigid amorphous fraction was found to develop in parallel to the crystal phase at low crystallization temperatures, whereas at higher T_c 's, RAF vitrification is observed only during the final stages of crystallization, in correspondence with the growth of secondary crystals. Investigation of the crystallization and melting behavior suggested the existence of a limit temperature for the formation and the disappearance of the rigid amorphous fraction in PLLA and PHB, which resulted approximately 130 and 70 °C, respectively [19–21]. At T_c 's higher than 130 °C, RAF was found not to develop at all during isothermal crystallization of PLLA. These limit temperatures were related to the mobility of the chains: at high crystallization temperatures, the polymer chains have high mobility, which facilitates the organization of the polymeric segments into ordered crystal structures, with reduced stress transmitted to the amorphous segments, and, in turn no or minor fraction of amorphous chain segments subjected to geometrical constraints. Conversely, the low chain mobility at low crystallization temperatures implies a more difficult organization of the entangled chain segments into ordered crystal structures, so that a larger rigid amorphous fraction develops. Full mobilization of the RAF upon heating was found to occur both for PLLA and PHB at the same temperature at which the RAF starts to develop upon crystallization. As regards PHB, the limit of 70 °C corresponds exactly to the temperature of complete

RAF devitrification reported by other authors, who located it in correspondence of the lowest melting peak [9, 10].

Recently, it was demonstrated that the limit temperature for the presence of the rigid amorphous fraction in poly(ethylene terephthalate) (PET) is around 210 °C [22]. Since its discovery, PET has been considered as a model polymer for the study of the properties of semirigid semicrystalline polymers, due to its low crystallization rate that allows to easily tune the crystalline fraction. The crystallization and melting behavior of PET has been the subject of many studies [23–37]. In particular, the effects of crystallization temperature, heating rate, crystallization time, and molar mass have been investigated, with the aim of explaining the origin of the multiple melting endotherms typical of PET [33–37].

A multiple melting behavior is commonly observed in semicrystalline polymers. Different reasons have been adduced to explain this behavior, such as the presence of more than one crystalline form [38], molar mass segregation during crystallization or annealing [39–41], fusion of crystals and confined nanocrystals [42, 43], orientation effects [44], and, more frequently, the occurrence of a melting/recrystallization/remelting process. The multiple melting behavior of PET is usually associated to the latter mechanism, which has been attributed to the fusion of original lamellae, followed by recrystallization and final fusion of the more perfect recrystallized crystals [24, 28, 33–37].

Although the mechanism has been identified, the connection between a specific thermal history and the appearance of a well resolved double or triple endotherm has not yet been sufficiently investigated. In the present study, for the first time, the effect of the rigid amorphous fraction on the melting behavior of PET is analyzed in detail and the triple and double melting endotherm explained as a consequence of the presence and absence of RAF in the original crystals, respectively.

Experimental methods

Poly(ethylene terephthalate) (PET) of molar mass $M_w = 21,400 \text{ g mol}^{-1}$, was kindly received through the Bank of Crystallizable Polymers of European funded COST Action P12. After drying under vacuum at 100 °C for 16 h, the sample chips were compression-molded with a Carver Laboratory Press at a temperature of 280 °C for 3 min, without any applied pressure, to allow complete melting. After this period, a pressure of about 100 bar was applied for 2 min. Successively, the sample was quickly cooled to room temperature by means of cold water circulating in the plates of the press. The thickness of the resulting film was about 200 μm .

Differential scanning calorimetry (DSC) and temperature-modulated calorimetry (TMDSC) measurements were performed with a PerkinElmer differential scanning calorimeter DSC 8500 equipped with an IntraCooler III as refrigerating

system. The instrument was calibrated in temperature with high purity standards (indium, naphthalene, cyclohexane) according to the procedure for standard DSC [45]. Energy calibration was performed with indium. In order to gain precise heat capacity data from the heat flow rate measurements, each scan was accompanied by an empty pan run and calibration with sapphire [45]. Dry nitrogen was used as purge gas at a rate of 30 mL min⁻¹. A fresh sample was employed for each analysis to minimize thermal degradation. In order to minimize temperature gradients, the PET sample mass was kept as small as possible, approximately 4 mg. All the results presented and discussed are the average of repeated runs. Before the analyses, each compression-molded PET sample was heated from room temperature to 280 °C at a rate of 50 °C min⁻¹ and maintained at this temperature for 3 min, in order to destroy completely the previous crystal order.

Isothermal crystallizations of PET were performed at various temperatures (180 °C ≤ T_c ≤ 230 °C) for a fixed time (60 min), as well as for the time sufficient to obtain the leveling of the heat flow rate signal after the exothermal peak. Isothermal crystallizations at 190, 200, 210, and 220 °C were also extended up to 10 h. All the samples had been previously melted for 3 min at 280 °C and quenched by ballistic cooling down to T_c . At the end of crystallization, in order to prevent further crystallization upon cooling, the samples were reheated at 5 or 10 °C min⁻¹ directly from T_c up to 280 °C.

TMDSC measurements were performed after isothermal crystallizations of 60 min at 200, 210, 220, and 230 °C. TMDSC analyses were designed using a sawtooth modulation temperature program. The temperature amplitude was 1.0 °C, the modulation period 60 s and the underlying heating rate 2 °C min⁻¹. The semi-period rates were +6.0 and -2.0 °C min⁻¹, respectively. According to the mathematical treatment of TMDSC data, the modulated temperature and the heat flow rate curves can be approximated to Fourier series and separated into underlying and periodic components [46–49]. The underlying components are equivalent to the conventional linear temperature program and the corresponding conventional DSC curve. The periodic components result from the difference between the respective modulated and underlying curves. The reversing specific heat capacity ($c_{p,rev}$) is obtained from the ratio between the amplitudes of the first harmonic of heat flow rate (A_{HF}) and temperature (A_T):

$$c_{p,rev}(\omega, T) = \frac{A_{HF}(T)K(\omega, T)}{A_T(T) m\omega} \quad (1)$$

where ω is the frequency of temperature modulation ($\omega=2\pi/p$) and m the mass of the sample. The frequency dependent calibration factor, $K(\omega, T)$, determined by calibration with sapphire, was 1.05 for $p=60$ s and 1.0 for $p=120$ s. The correctness of the calibration factor was proven by the good

agreement between the PET measured specific heat capacity and the thermodynamic liquid specific heat capacity data [50].

Annealing studies were performed on PET samples non-isothermally crystallized at -10 °C min⁻¹ from 280 °C down to 50 °C, after fusion for 3 min at 280 °C. The samples were reheated at 10 °C min⁻¹ from 50 °C up to various annealing temperatures (190 °C ≤ T_a ≤ 230 °C) and maintained at T_a for 60 min, then again reheated at 10 °C min⁻¹ directly from T_a up to 280 °C by conventional DSC.

Results and discussion

Isothermal crystallizations and melting

Isothermal crystallizations of PET were performed at different temperatures, specifically between 180 and 230 °C, i.e., above and below the limit temperature for the presence of RAF in PET, which is around 210 °C [22], and the successive melting behavior was monitored in dependence of T_c . Isothermal crystallizations were performed at each T_c (*i*) for 60 min and (*ii*) for the time strictly needed to obtain the leveling of the heat flow rate signal after the exothermal peak. After isothermal crystallization, PET was heated at 10 °C min⁻¹ up to complete fusion. PET samples isothermally crystallized for 60 min were also melted at 5 °C min⁻¹.

With changing the crystallization temperature, some variations in the successive melting behavior can be observed, as exemplified in Figs. 1 and 2. Figure 1 presents the apparent specific heat capacity ($c_{p,app}$) of PET recorded at 5 and 10 °C min⁻¹ immediately after the isothermal crystallizations at the various T_c 's for 60 min, whereas Fig. 2 collects the $c_{p,app}$ curves at 10 °C min⁻¹ after the isothermal crystallizations at the various T_c 's for 60 min and for the time needed to obtain the leveling of the heat flow rate signal after the exothermal peak. A multiple melting behavior can be observed in all the $c_{p,app}$ curves, in agreement with literature data [24, 30, 33, 36]. Samples crystallized at $T_c \leq 215$ °C exhibit three endotherms of different relative intensity, whereas samples crystallized at $T_c > 215$ °C display only two peaks, independently of both crystallization time and scanning rate. The endotherms are labeled I, II, and III in order of increasing temperatures, as shown in Figs 1 and 2.

Endotherm I moves to higher temperature with increasing T_c and crystallization time. Its intensity is small for $T_c \leq 215$ °C and progressively increases at $T_c > 215$ °C, becoming comparable with the second peak after crystallization at 220 °C. Endotherm I, observed in PET and in other polymers approximately 10–20 °C above T_c , is generally associated with the fusion of defective secondary lamellae, which grow in the presence of more perfect crystals during secondary crystallization and melt earlier because of their lower stability [33, 36, 51]. It has also been attributed to the onset of the overall

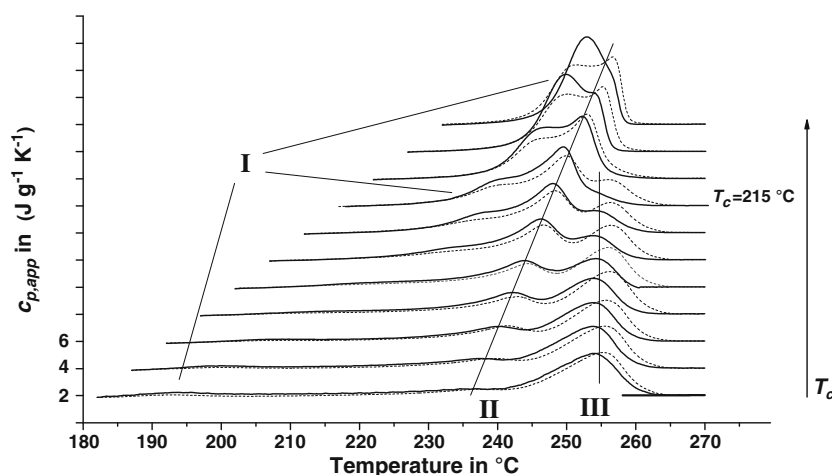


Fig. 1 Apparent specific heat capacity ($c_{p,app}$) of PET upon heating at 5 °C min^{-1} (dotted lines) and 10 °C min^{-1} (solid lines) after isothermal crystallization at $T_c=180, 185, 190, 195, 200, 205, 210, 215, 220, 225,$ and 230 °C for 60 min. The ordinate values refer only to the bottom curve ($T_c=180\text{ °C}$). All the other curves are shifted vertically for the sake

of clearness. The thin black solid lines serve as guides for the eyes, to evidence the location of the endothermic events labeled I, II, and III. The thick solid line is the thermodynamic liquid specific heat capacity of PET [50]

melting process, being this melting partially masked by the concomitant recrystallization [37]. Its intensity and location strongly depends on the crystallization time (t_c), especially at high T_c . The second melting peak (II) increases in size and moves to higher temperatures with increasing T_c . Its intensity is a function also of the crystallization time. Endotherm II becomes progressively more pronounced with increasing t_c up to about $T_c=210\text{ °C}$; after crystallization at higher temperatures, its intensity results progressively less dependent on t_c . This endothermic event has been associated to the fusion of crystals grown at T_c by primary crystallization [30, 36]. Conversely, endotherm III has been attributed to the melting of lamellae fully recrystallized upon heating [30, 36]. Its location

is approximately independent of T_c , but dependent on the heating rate, as it shifts to higher temperatures with reducing the heating rate, in agreement with literature data [36]. The ratio of the area of endotherm III to the area of endotherm II increases (i) with reducing the heating rate, as more time is available for recrystallization/reorganization, (ii) with reducing T_c , because of the less perfect original crystals, and (iii) with reducing t_c , which attests that a reorganization/perfecting process occurs during the isothermal crystallization. After crystallization at 220 °C endotherm III is fully disappeared.

The effect of t_c on PET melting behavior was further investigated at $190, 200, 210,$ and 220 °C by prolonging the crystallization time up to 10 h. Figure 3 shows that endotherm

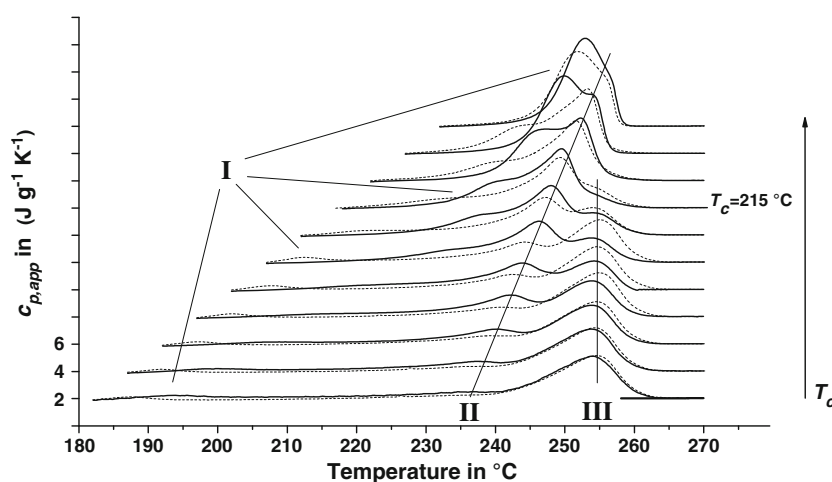
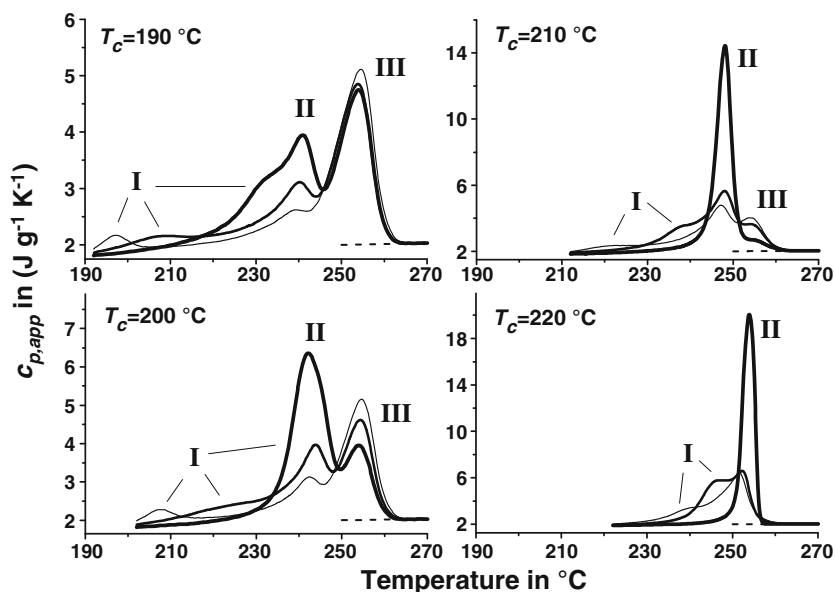


Fig. 2 Apparent specific heat capacity ($c_{p,app}$) of PET upon heating at 10 °C min^{-1} after isothermal crystallization at $T_c=180, 185, 190, 195, 200, 205, 210, 215, 220, 225,$ and 230 °C for 60 min (solid lines) and for 6, 6, 7, 8, 9, 10, 15, 20, 25, 30, and 45 min, respectively (dotted lines). The ordinate values refer only to the bottom curve ($T_c=180\text{ °C}$). All the other

curves are shifted vertically for the sake of clearness. The thin black solid lines serve as guides for the eyes, to evidence the location of the endothermic events labeled I, II, and III. The thick solid line is the thermodynamic liquid specific heat capacity of PET [50]

Fig. 3 Apparent specific heat capacity ($c_{p,app}$) of PET upon heating at $10\text{ }^{\circ}\text{C min}^{-1}$ after isothermal crystallization at $T_c=190, 200, 210,$ and $220\text{ }^{\circ}\text{C}$ for 10 h (thick solid line), 60 min (solid line), and 7, 9, 15, and 25 min, respectively (thin solid line). The dashed lines are the thermodynamic liquid specific heat capacity of PET [50]



I moves to higher temperatures after 10 h of isothermal crystallization: after crystallization at $190\text{ }^{\circ}\text{C}$, it appears as a shoulder on the low temperature side of endotherm II, whereas after crystallization at higher T_c 's, it progressively merges with endotherm II, as evidenced by the asymmetry of peak II after crystallization at $200\text{ }^{\circ}\text{C}$. Endotherm II increases markedly after 10 h of isothermal crystallization and shifts to slightly higher temperatures after crystallization at $220\text{ }^{\circ}\text{C}$. Also, endotherm III is affected by the preceding thermal treatment: its intensity reduces progressively with increasing both T_c and t_c . After 10 h of isothermal crystallization at $210\text{ }^{\circ}\text{C}$, endotherm III practically disappears. Prolonged crystallization at $220\text{ }^{\circ}\text{C}$ results in a single narrow melting endotherm.

Experimental evidences from fast calorimetry proved that isothermal crystallization leads to a monomodal distribution of lamellar thickness [37]. Moreover, PET does not display crystal polymorphism upon crystallization from isotropic melt [24]. Why after crystallization at T_c lower than $215\text{ }^{\circ}\text{C}$, besides peak I, two different and well-resolved peaks (II and III) are detected during the melting/recrystallization/remelting process of PET at conventional heating rate, whereas after crystallization at higher T_c 's, only one peak (II) is observed, it has not yet been explained in detail and satisfactorily as regards the morphology and the reorganization mechanism.

Isothermal crystallizations and TMDSC heating

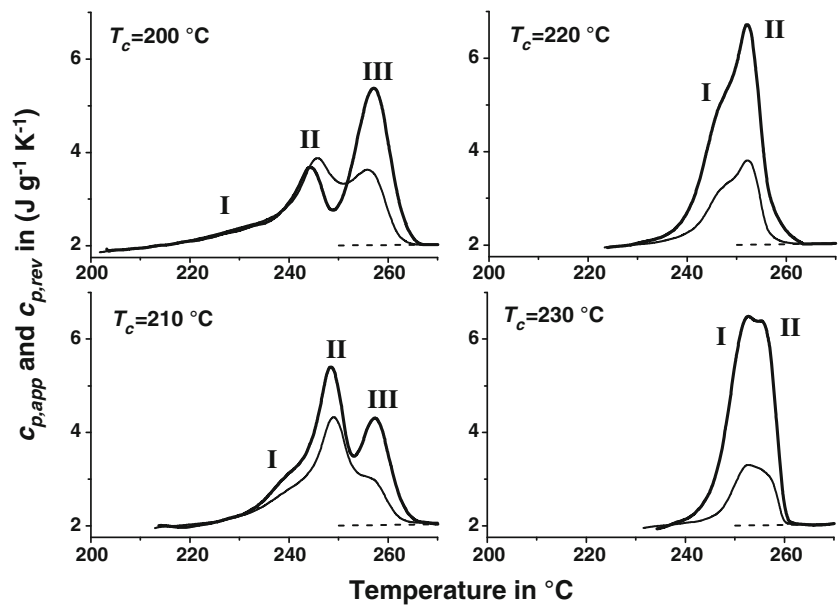
In an attempt to gain further insight into the melting-recrystallization-remelting process occurring during PET heating, TMDSC analyses were performed on samples isothermally crystallized for 60 min at $200, 210, 220,$ and $230\text{ }^{\circ}\text{C}$. With the temperature modulated technique, multiple signals are generated in a single experiment, so that each of the

components of the conventional heat flow rate curve can be identified and separated.

Figure 4 displays the apparent specific heat capacity ($c_{p,app}$) and the reversing specific heat capacity ($c_{p,rev}$), measured with $p=60\text{ s}$, after isothermal crystallization at temperatures below and above the critical T_c of $215\text{ }^{\circ}\text{C}$. The shape of the $c_{p,rev}$ and $c_{p,app}$ curves is similar, but the intensity of the respective peaks is different. In particular, the intensity of the $c_{p,rev}$ peak III, after crystallization at 200 and $210\text{ }^{\circ}\text{C}$, and the intensity of the entire $c_{p,rev}$ curve, after crystallization at 220 and $230\text{ }^{\circ}\text{C}$, result markedly reduced with respect to the corresponding $c_{p,app}$ values. This indicates that fusion of the crystals, grown during isothermal crystallization at high T_c or perfected during the modulated heating run with $p=60\text{ s}$, is partially irreversible and that the simultaneous recrystallization of these crystals occurs to a minor extent. This derives from the fact that the amplitude of modulated heat flow originates from the sum of the absolute values of the endothermic and exothermic event intensity occurring within each modulation period, whereas the latent heat released or absorbed sum algebraically when the apparent specific heat capacity is determined [18, 49]. Conversely, with reducing perfection of the primary crystals, the recrystallization degree increases, as attested by the intensity of the $c_{p,rev}$ peak II after crystallization at $200\text{ }^{\circ}\text{C}$, which is higher than the corresponding $c_{p,app}$ endotherm II. This finding is in agreement with literature data [52–54]. It has been reported for different polymers that less perfect crystals undergo reversing melting to a higher extent with respect to more perfect crystals, as recrystallization of poor crystals is subjected to minor restrictions.

It is worthwhile to analyze also the periodic heat flow rate curves (HF_p), which are reported in Fig. 5. The TMDSC data are presented to show that the double melting behavior

Fig. 4 Apparent specific heat capacity ($c_{p,app}$) (thick line) and reversing specific heat capacity ($c_{p,rev}$) ($A_T=1.0\text{ }^\circ\text{C}$, $p=60\text{ s}$) (thin line) of PET upon heating at $+2\text{ }^\circ\text{C min}^{-1}$ after isothermal crystallization for 60 min at 200, 210, 220, and 230 $^\circ\text{C}$. The dashed lines are the thermodynamic liquid specific heat capacity of PET [50]

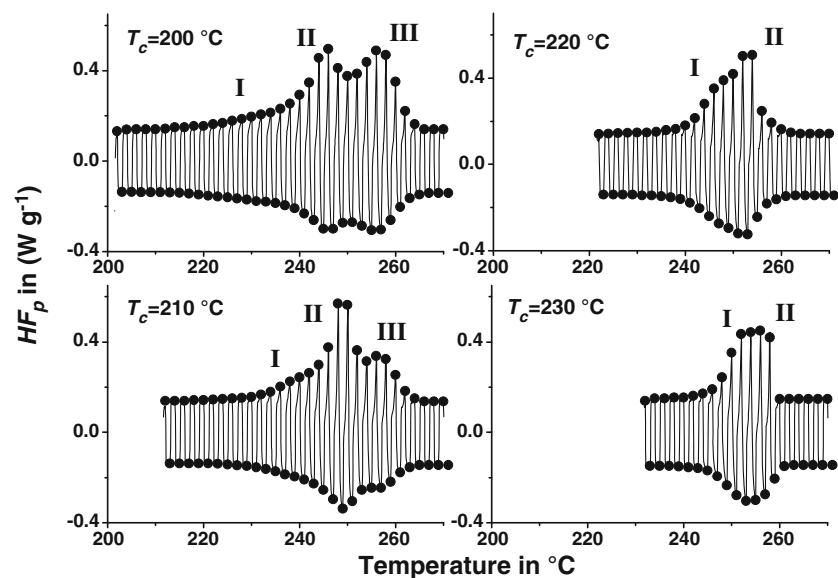


displayed by the $c_{p,app}$ curves can be observed also in the concomitant recrystallization. The periodic heat flow rate comprises only the thermal events that take place within the time scale of the temperature modulation and are reversed by it. In this way, opposite events, as for example melting and recrystallization, can be highlighted individually, as they take place separately in the heating and cooling semiperiods, respectively.

The HF_p curves show that fusion and recrystallization occur distinctly already from 15 $^\circ\text{C}$ above T_c , as attested by the progressively increasing endothermic and exothermic signals, which involve at first the reorganization of the less perfect secondary crystals. After crystallization at 200 and 210 $^\circ\text{C}$, two well-resolved melting peaks can be observed

during the heating semiperiods in correspondence of endotherms II and III, as well as two recrystallization peaks during the corresponding cooling semiperiods. Conversely, after crystallization at 220 and 230 $^\circ\text{C}$, less resolved double melting and recrystallization processes, originating from the merging of peak I with peak II, are displayed by the periodic heat flow. Neglecting the reorganization of the more defective secondary crystals, connected to peak I, the fact that fusion and recrystallization proceed through two different and separated paths after crystallization at $T_c < 215\text{ }^\circ\text{C}$, suggests that two different primary crystalline organizations develop during isothermal crystallization at $T_c < 215\text{ }^\circ\text{C}$, in a percentage that is a function of the crystallization temperature. These two different morphologies differently transform upon heating at low scanning

Fig. 5 Periodic heat flow rate curves (HF_p) of PET upon heating at $+2\text{ }^\circ\text{C min}^{-1}$ after isothermal crystallization for 60 min at 200, 210, 220 and 230 ($A_T=1.0\text{ }^\circ\text{C}$, $p=60\text{ s}$). The solid circles outline the envelopes of the maximum and minimum values of the periodic heat flow rate in the heating and cooling semiperiods



rate, originating endotherms II and III. On the contrary, after crystallization at $T_c > 215$ °C, a single reorganization route is followed by all the primary crystalline structures, which probably are characterized by the same morphology.

It is well known that morphological features of crystallizable polymers are controlled by kinetic factors and that changes in the molecular rearrangements and morphological superstructure are expected as a function of the crystallization conditions. Crystallization of semiflexible chain polymers, such as PET cannot always involve tight adjacent reentry folding, because of local chain rigidity. According to literature data, morphology of PET crystals varies with temperature of formation. At very low crystallization temperatures ($T_c = 100$ °C), crystals without lamellar structure were observed, probably consisting of chain cluster aggregation [24]. At a higher crystallization temperature ($T_c = 150$ °C), highly branched lamellae with small lateral dimensions were detected, whereas at $T_c = 220$ °C, the typical lamellar structure was observed [24].

Small-angle X-ray scattering and wide-angle X-ray diffraction studies on PET samples heated and annealed above the crystallization temperatures showed a change in structural parameters around 215 °C [26, 28]. A discontinuity in the reorganization mechanism was conjectured, though with different scenarios. Jonas et al. suggested that, upon heating, the average thickness of the crystalline lamellae increases markedly and dramatically above 215 °C [28], whereas Fontaine et al. hypothesized that crystal reorganization during annealing occurs via crystal thickening below 215 °C and via crystal perfection at the amorphous/crystal boundaries above 215 °C [26].

As illustrated in Figs. 1–2, PET crystallization at $T_c < 215$ °C leads to triple melting endotherms, whereas crystals grown at $T_c > 215$ °C display a double melting behavior upon heating at conventional DSC rates. The transition temperature from the triple to the double melting behavior of the analyzed PET sample, 215 °C, is very close to the limit temperature for the presence of the rigid amorphous fraction in PET, which is around 210 °C [22]. This leads to hypothesize a possible influence of the RAF on the multiple melting behavior of PET.

The discontinuity in the melting behavior after crystallization at temperatures lower and higher than 215 °C can be rationalized by considering that PET crystallization at temperatures lower than 215 °C is accompanied by partial vitrification of the amorphous chain portions in proximity of the crystal domains, in a percentage that increases with decreasing T_c [19, 21]. Temperature is closely related to the mobility of polymer chains: at high T_c , the polymer chains have high mobility, which facilitates organization of the polymeric segments into ordered crystal structures, with high percentage of tight adjacent reentry folding and no stress transmitted to the amorphous segments, which corresponds to the absence of rigid amorphous fraction. With decreasing T_c , the percentage

of defective crystalline structures, constituted by small crystalline domains and chain cluster aggregations, increases progressively, accompanied by an increasing fraction of amorphous chain segments subjected to geometrical constraints (see Fig. 6).

During the heating that follows isothermal crystallization at $T_c < 215$ °C, the RAF devitrification that occurs simultaneously with the melting of chain cluster aggregates, can favor the rearrangements needed to form more ordered structure, and as a consequence, to promote recrystallization and/or additional crystallization, particularly at the amorphous/crystal boundaries. This results in an increased crystal thickness and in a higher thermal stability of crystals with larger dimensions, which undergo fusion at higher temperatures, originating endotherm III. Also, the more perfect crystalline regions, whose fraction increases with T_c , constituted by crystals grown with a high percentage of adjacent reentry folding and reduced constraints on their boundaries, can melt/recrystallize and reorganize during the heating scan. In this case, the positive action exerted by the RAF concerted mobilization is absent, which results in a slightly lower melting temperature (endotherm II), as fusion and recrystallization of chain folded lamellae is a multistep process that requires the detachment of all the crystalline stems, their diffusion towards other amorphous segments, and their successive ordering into a new thicker crystalline structure. The process is expected to be faster the smaller the lateral dimensions of the lamellae. As a consequence of the high mobility of the PET polymer segments, crystallizations conducted at $T_c > 215$ °C possibly take place without development of RAF, as evidenced by the full disappearance of endotherm III. The reorganization process during heating could involve mostly crystals perfection through the annihilation of defects inside the lamellae or at the interfaces of the crystalline regions. A tentative pictorial representation of the possible effects of heating on the morphology of the crystal/amorphous interface is given in Fig. 6.

A confirmation that different reorganization mechanisms operate during heating is given in the literature for isotactic polystyrene (iPS), which, as PET, exhibits triple or double melting behavior [55]. Small-angle X-ray scattering measurements revealed no evident change in the crystal thickness up to final melting after crystallization at temperatures higher than 220 °C, whereas gradual increase in crystal thickness was detected after crystallization at lower temperatures. The limit crystallization temperature of 220 °C corresponds exactly to the transition between triple and double melting behavior in iPS [52]. These results lead to hypothesize that similar reorganization mechanisms are active in PET and iPS, being both PET and iPS characterized by semirigid chains, with bulky moieties in the backbone and as side groups, respectively.

A proof of the connection between crystalline morphology and melting behavior has been reported for poly(ethylene

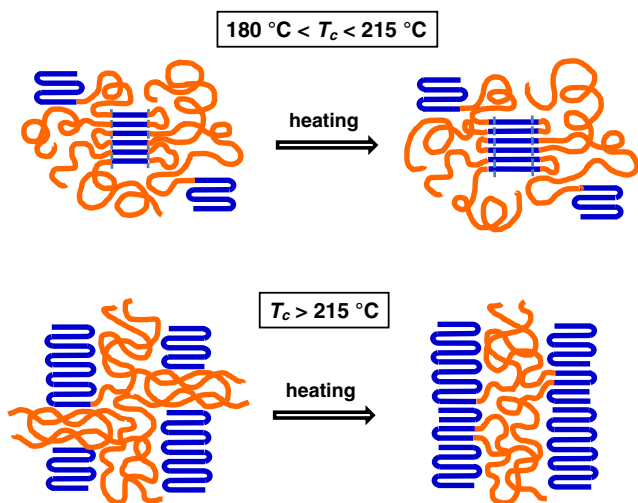


Fig. 6 Tentative schematic model for the reorganization process upon heating in PET

naphthalene-2,6-dicarboxylate) (PEN), a semirigid polyester similar to PET, containing naphthalene instead of benzene rings in the main chain [56]. PEN exhibits a multiple melting behavior which depends, as for PET, on the crystallization temperature. Small-angle X-ray scattering measurements proved that the dual melting endotherm corresponds to a morphology which is best described by a dual lamellar stack model, with lamellae of different thickness in separate stacks, whereas the single melting peak was found to correspond to a more homogenous distribution of lamellar thickness [56]. These experimental results obtained for PEN are in agreement with the different crystalline morphologies that are here proposed for PET as a function of the crystallization temperature.

Crystallization time plays an important role on the development of the crystalline phase. An increase in t_c raises the crystalline fraction and allows the development of more perfect crystalline areas through the removal of crystal imperfections and a better delimitation at the amorphous/crystal interfaces. The higher the time allowed for the arrangement of the polymer segments into ordered structure, the smaller the layer of immobilized amorphous segments around the crystals, as attested by the increased intensity of endotherm II, and by the lower intensity of endotherm III (see Fig. 2). Also, endotherm I, associated with the fusion of more defective secondary crystallites, becomes more pronounced and moves to higher temperatures with increasing t_c . The change is much more pronounced at higher crystallization temperatures, as the progressive reduction of RAF favors crystallization of the amorphous segments into ordered structures also in geometrically more restricted areas. After crystallization for 10 h at $T_c \geq 210$ °C, endotherm I has completely merged with endotherm II into a single narrow peak, attesting that after long crystallization times, primary and secondary crystals are almost equivalent, as the rigid amorphous fraction is completely absent.

Non-isothermal crystallization, annealing, and melting

With the aim to further highlight how the thermal history influences the melting behavior, PET was non-isothermally crystallized at -10 °C min^{-1} . The crystallization peak is centered around 200 °C, as illustrated in the inset of Fig. 7, which means that RAF should develop during part of the non-isothermal crystallization. The samples were then heated at 10 °C min^{-1} up to annealing temperatures in the range 190 °C $\leq T_a \leq 230$ °C and maintained at T_a for 60 min. The successive melting behavior is illustrated in Fig. 7.

All the $c_{p,app}$ curves exhibit three endotherms. Endotherm I moves to higher temperatures and markedly increases in intensity after annealing at $T_a \leq 215$ °C. Endotherm II remains substantially unchanged after annealing at $T_a \leq 210$ °C, but it is no more detectable after annealing at $T_a > 210$ °C, likely because it is masked or included within endotherm I. Endotherm III slightly reduces with increasing T_a , but it does not disappear, which means that the reorganization during annealing partially involves also the original crystalline chain cluster aggregations. As stated above, peak II derives from recrystallization/reorganization of the preexisting primary crystalline regions constituted by folded lamellae, whereas peak III is the result of recrystallization of preexisting primary crystalline domains made of chain cluster aggregations with a high percentage of rigid amorphous fraction on the boundaries.

The progressive rise of endotherm I attests the increase in the secondary crystal growth during annealing. This increase is more marked after annealing at $T_a \geq 215$ °C, suggesting that a change in the crystallization mechanism or kinetics takes

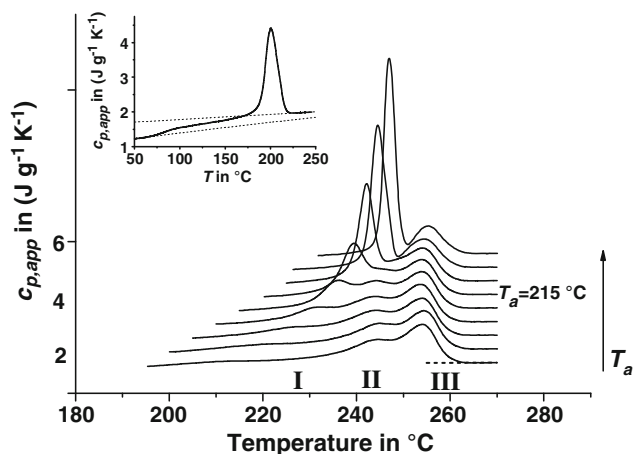


Fig. 7 Apparent specific heat capacity ($c_{p,app}$) of PET upon heating at 10 °C min^{-1} after non-isothermal crystallization at -10 °C min^{-1} and annealing for 60 min at $T_a = 190, 195, 200, 205, 210, 215, 220, 225,$ and 230 °C. The ordinate values refer only to the bottom curve ($T_a = 190$ °C). All the other curves are shifted vertically for the sake of clearness. In the inset, the apparent specific heat capacity ($c_{p,app}$) of PET upon cooling from the melt at -10 °C min^{-1} is reported. The dotted lines are the thermodynamic specific heat capacities of PET [50]

place around this temperature. This finding is in excellent agreement with the results discussed above: secondary crystallization is permitted to large extent at temperatures higher than 215 °C, because of the absence of rigid amorphous fraction and therefore of constraints for the rearrangement of the polymeric amorphous segments into more ordered crystalline structures. It is worth to note that a discontinuity in the reversing heat capacity of PET was recently observed after annealing at 210 °C [22] that is at temperature very close to the limit temperature of 215 °C identified in the present study. The results were rationalized by hypothesizing that below 210 °C, the vitrified RAF hinders crystal reorganization and perfection during annealing, whereas above 210 °C, the strain of the amorphous chains coupled with the crystals is released, so that a larger crystal fraction undergo reorganization and reversing melting, which determines the varied reversing heat capacity.

Conclusions

In order to verify the possible existence of a limit temperature for the presence of the rigid amorphous fraction in PET, the effects of isothermal crystallizations and annealing treatments on the melting behavior were studied and analyzed by conventional and temperature-modulated differential scanning calorimetry.

The multiple melting behavior of PET is generally attributed to the fusion of original crystals recrystallized during heating at low and conventional DSC scanning rates. In the present study, the double and triple melting behavior that is observed after isothermal crystallization at T_c higher and lower than 215 °C, respectively, have been put in relation with the absence and presence of vitrified rigid amorphous portions coupled to original crystals. The discontinuity in thermal behavior observed after crystallization at temperatures lower and higher than 215 °C has been rationalized by assuming that PET crystallization at temperatures lower than 215 °C is accompanied by partial vitrification of the amorphous chain portions in proximity of the crystal lamellae. RAF vitrification depends on chain mobility, which in turn is closely connected to the isothermal crystallization temperature: a lower chain mobility complicates the organization of the entangled chain segments into ordered crystal structures, so that a larger rigid amorphous fraction develops. Conversely, at high T_c , the polymer chains have high mobility, which facilitates the organization of the polymeric segments into ordered crystal structures, with reduced stress transmitted to the amorphous segments and, in turn, a lower fraction of chain segments subjected to geometrical constraints.

The complex melting behavior detected after isothermal crystallization has been explained by assuming that two different primary morphologies develop during crystallization at $180\text{ °C} < T_c < 215\text{ °C}$, in a percentage that is a function of the

crystallization temperature. The less perfect primary morphology is constituted by small crystalline domains made of chain cluster aggregations, with a high fraction of coupled rigid amorphous segments. Conversely, the more perfect primary crystalline regions, whose percentage increases with T_c , originate from crystals with a high fraction of adjacent reentry folding and reduced constraints at the amorphous/crystal interface. These two distinct morphologies differently transform upon heating at low scanning rate, originating endotherms II and III. On the contrary, after crystallization at $T_c > 215\text{ °C}$, a single reorganization route is followed by all the primary crystalline structures, which probably are characterized by the same morphology made of tightly chain folded lamellae.

References

1. Wunderlich B (2005) Thermal analysis of polymeric materials. Springer, New York
2. Wunderlich B (2003) Reversible crystallization and the rigid amorphous phase in semicrystalline macromolecules. *Prog Polym Sci* 28: 383–450
3. Di Lorenzo ML, Righetti MC (2008) The three-phase structure of isotactic poly(1-butene). *Polymer* 49:1323–1331
4. Martin S, Exposito MT, Vega JF, Martinez-Salazar J (2013) Microstructure and properties of branched polyethylene: application of a three-phase structural model. *J Appl Polym Sci* 128:1871–1878
5. Lin J, Shenogin S, Nazarenko S (2002) Oxygen solubility and specific volume of rigid amorphous fraction in semicrystalline poly(ethylene terephthalate). *Polymer* 43:4733–4743
6. Guinault A, Sollogoub C, Ducruet V, Domenek S (2012) Impact of crystallinity of poly(lactide) on helium and oxygen barrier properties. *Eur Polym J* 48:779–788
7. Kolesov I, Androsch R (2012) The rigid amorphous fraction of cold-crystallized polyamide 6. *Polymer* 53:4770–4777
8. Delpouve N, Stoclet G, Saiter A, Dargent E, Marais S (2012) Water barrier properties in biaxially drawn poly(lactic acid) films. *J Phys Chem B* 16:4615–4625
9. Schick C, Wurm A, Mohamed A (2001) Vitrification and devitrification of the rigid amorphous fraction of semicrystalline polymers revealed from frequency-dependent heat capacity. *Colloid Polym Sci* 279:800–806
10. Schick C, Wurm A, Mohammed A (2003) Formation and disappearance of the rigid amorphous fraction in semicrystalline polymers revealed from frequency dependent heat capacity. *Thermochim Acta* 396:119–132
11. Xu X, Ince S, Cebe P (2003) Development of the crystallinity and rigid amorphous fraction in cold-crystallized isotactic polystyrene. *J Polym Sci Polym Phys* 41:3026–3036
12. Xu H, Cebe P (2004) Heat capacity study of isotactic polystyrene: dual reversing crystal melting and relaxation of rigid amorphous fraction. *Macromolecules* 37:2797–2806
13. Righetti MC, Tombari E, Di Lorenzo ML (2008) Crystalline, mobile amorphous and rigid amorphous fractions in isotactic polystyrene. *Eur Polym J* 44:2659–26676
14. Androsch R, Wunderlich B (2005) The link between rigid amorphous fraction and crystal perfection in cold-crystallized poly(ethylene terephthalate). *Polymer* 46:12556–12566
15. Righetti MC, Tombari E, Angiuli M, Di Lorenzo ML (2007) Enthalpy-based determination of crystalline, mobile amorphous and

- rigid amorphous fractions in semicrystalline polymers: poly(ethylene terephthalate). *Thermochim Acta* 462:15–24
16. Chen H, Cebe P (2009) Vitrification and devitrification of rigid amorphous fraction of PET during quasi-isothermal cooling and heating. *Macromolecules* 42:288–292
 17. Ma Q, Georgiev G, Cebe P (2011) Constraints in semicrystalline polymers: using quasi-isothermal analysis to investigate the mechanisms of formation and loss of the rigid amorphous fraction. *Polymer* 52:4562–4570
 18. Righetti MC, Di Lorenzo ML, Tombari E, Angiuli M (2008) The low-temperature endotherm in poly(ethylene terephthalate): partial melting and rigid amorphous fraction mobilization. *J Phys Chem B* 112:4233–4241
 19. Righetti MC, Tombari E (2011) Crystalline, mobile amorphous and rigid amorphous fractions in poly(L-lactic acid) by TMDSC. *Thermochim Acta* 522:118–127
 20. Di Lorenzo ML, Gazzano M, Righetti MC (2012) The role of the rigid amorphous fraction on cold crystallization of poly(3-hydroxybutyrate). *Macromolecules* 45:5684–5691
 21. Righetti MC, Tombari E, Di Lorenzo ML (2013) The role of the crystallization temperature on the nanophase structure evolution of poly[(R)-3-hydroxybutyrate]. *J Phys Chem B* 117:12303–12311
 22. Di Lorenzo ML, Righetti MC, Cocca M, Wunderlich B (2010) Coupling between crystal melting and rigid amorphous fraction mobilization in poly(ethylene terephthalate). *Macromolecules* 43:7689–7694
 23. Bicerano J (1998) Crystallization of polypropylene and poly(ethylene terephthalate). *J Macromol Sci C Polym Rev J* 38:391–479
 24. Groeninckx G, Reynaers H, Berghmans H, Smets G (1980) Morphological and melting behaviour of semicrystalline poly(ethylene terephthalate) I isothermally crystallized PET. *J Polym Sci Polym Phys Ed* 18:1311–1324
 25. Groeninckx G, Reynaers H (1980) Morphological and melting behaviour of semicrystalline poly(ethylene terephthalate) II annealed PET. *J Polym Sci Polym Phys Ed* 18:1325–1341
 26. Fontaine F, Ledent J, Groeninckx G, Reynaers H (1982) Morphological and melting behaviour of semicrystalline poly(ethylene terephthalate): 3. Quantification of crystal perfection and crystallinity. *Polymer* 23:185–191
 27. Alfonso GC, Pedemonte E, Ponzetti L (1979) Mechanism of densification and crystal perfection of poly(ethylene terephthalate). *Polymer* 20:104–112
 28. Jonas AM, Russell TP, Yoon DY (1994) Time resolved SAXS studies of morphological changes in cold crystallized poly(ethylene terephthalate) during annealing and heating. *Colloid Polym Sci* 272:1344–1351
 29. Ivanov DA, Pop T, Yoon DY, Jonas AM (2002) Direct observation of crystal-amorphous interphase in lamellar semicrystalline poly(ethylene terephthalate). *Macromolecules* 35:9813–9818
 30. Wang Z-G, Hsiao BS, Sauer BB, Kampert WG (1999) The nature of secondary crystallization in poly(ethylene terephthalate). *Polymer* 40:4615–4627
 31. Alvarez C, Šics I, Nogales A, Denchev Z, Funari SS, Ezquerra TA (2004) Structure-dynamics relationship in crystallizing poly(ethylene terephthalate) as revealed by time-resolved X-ray and dielectric methods. *Polymer* 45:3953–3959
 32. Flores A, Pieruccini M, Nöchel U, Stribeck N, Baltà Calleja FJ (2008) Recrystallization studies on isotropic cold-crystallized PET: influence of heating rate. *Polymer* 49:965–973
 33. Zhou C, Clough SB (1988) Multiple melting endotherms of poly(ethylene terephthalate). *Polym Eng Sci* 28:65–68
 34. Lu XF, Hay JN (2001) Isothermal crystallization and melting behaviour of poly(ethylene terephthalate). *Polymer* 42:9323–9431
 35. Medellín-Rodríguez FJ, Phillips PJ, Lin JS, Campos R (1997) The triple melting behaviour of poly(ethylene terephthalate): molecular weight effects. *J Polym Sci B Polym Phys* 35:1757–1774
 36. Kong Y, Hay JN (2003) Multiple melting behaviour of poly(ethylene terephthalate). *Polymer* 44:623–633
 37. Minakov AA, Mordvintsev DA, Tol R, Schick C (2006) Melting and reorganization of the crystalline fraction and relaxation of the rigid amorphous fraction of isotactic polystyrene on fast heating (30, 000 K/min). *Thermochim Acta* 442:25–30
 38. Pan P, Inoue Y (2009) Polymorphism and isomorphism in biodegradable polyesters. *Prog Polym Sci* 34:605–640
 39. Müller AJ, Amal ML (2005) Thermal fractionation of polymers. *Prog Polym Sci* 30:559–603
 40. Righetti MC, Laus M (2000) The biphasic behaviour of a thermotropic polymeric polymeric polyester I. Time evolution of phase separation. *Polymer* 41:8355–8362
 41. Righetti MC, Laus M (2001) Biphasic behaviour of a thermotropic polymeric polymeric polyester II. Temperature evolution of phase separation. *Macromolecules* 34:7190–7196
 42. Giani E, Sparnacci K, Laus M, Palamone G, Kapeliouchko V, Arcella V (2003) PTFE-polystyrene core-shell nanospheres and nanocomposites. *Macromolecules* 36:4360–4367
 43. Righetti MC, Boggioni A, Laus M, Antonioli D, Sparnacci K, Boarino L (2013) Thermal and mechanical properties of PES/PTFE composites and nanocomposites. *J Appl Polym Sci* 130:3624–3633
 44. Capaccio G, Ward IM (1974) Preparation of ultra-high modulus linear polyethylenes; effect of molecular weight and molecular weight distribution on drawing behaviour and mechanical properties. *Polymer* 15:233–238
 45. Sarge SM, Hemminger W, Gmelin E, Höhne GWH, Cammenga HK, Eysel W (1997) Metrologically bases procedures for the temperature, heat and heat flow rate calibration of DSC. *J Therm Anal* 49:1125–1134
 46. Wunderlich B (1997) Modeling the heat flow and heat capacity of modulated differential scanning calorimetry. *J Therm Anal* 48:207–224
 47. Wurm A, Merzlyakov M, Schick C (1998) Reversible melting probed by temperature modulated dynamic mechanical and calorimetric measurements. *Colloid Polym Sci* 276:289–296
 48. Androsch R, Moon I, Kreitmeier S, Wunderlich B (2000) Determination of heat capacity with a sawtooth-type, power compensated temperature modulated DSC. *Thermochim Acta* 357–358:267–278
 49. Di Lorenzo ML, Wunderlich B (2003) Melting of polymers by non-isothermal, temperature-modulated calorimetry: analysis of various irreversible latent heat contributions to the reversing heat capacity. *Thermochim Acta* 405:255–268
 50. ATHAS Data Bank, M. Pyda M. (Ed.), Web address: <http://www.springermaterials.com/docs/athas.html>
 51. Righetti MC, Di Lorenzo ML (2011) Melting temperature evolution of non-reorganized crystals. Poly(3-hydroxybutyrate). *Thermochim Acta* 512:59–66
 52. Schick C, Merzlyakov M, Wunderlich B (1998) Analysis of the reorganization of poly(ethylene terephthalate) in the melting range by temperature-modulated calorimetry. *Polym Bull* 40:297–303
 53. Ishikiriyama K, Wunderlich B (1997) Melting of poly(oxyethylene) analyzed by temperature-modulated calorimetry. *Macromolecules* 30:4126–4131
 54. Righetti MC (1999) Reversible melting in poly(butylene terephthalate). *Thermochim Acta* 330:131–135
 55. Al-Hussein M, Strobl G (2002) The melting line, the crystallization line, and the equilibrium melting temperature of isotactic polystyrene. *Macromolecules* 35:1672–1676
 56. Denchev Z, Nagales A, Ezquerra TA, Fernandes-Nascimento J, Baltà-Calleja FJ (2000) On the origin of the multiple melting behaviour in poly(ethylene naphthalate-2,6-dicarboxylate): microstructural study as revealed by differential scanning calorimetry and x-ray scattering. *J Polym Sci B Polym Phys* 38:1167–1182